RSC Sustainability

ROYAL SOCIETY OF CHEMISTRY

PAPER

View Article Online
View Journal | View Issue

Open Access Article. Published on 27 October 2025. Downloaded on 1/13/2026 2:20:04 AM.
This article is licensed under a Creative Commons Attribution-NonCommercial 3.0 Unported Licence.

Check for updates

Cite this: *RSC Sustainability*, 2025, **3**, 5653

Assessing the environmental footprint of electrochromic windows: a comparative LCA with AI-based forecasting

Mohsen Rabbani,[a] Olivia Tahti,[b] Sabinus Essel Arthur,[a] Macy A. Hopping,[c] Christopher J. Barile,[c] Mohd Hassan Karim,[d] Ario Fahimi[e] and Ehsan Vahidi *[a]

This investigation assesses electrochromic windows as a novel green alternative to traditional double-pane windows through a life cycle assessment, which analyzes and compares both types of windows. The life cycle assessment was conducted using the impact categories of TRACI 2.1 in the SimaPro 9.1 application, with ecoinvent, and 1 m^2 of each window type as the functional unit for the comparisons. The manufacturing of EC windows yielded a total CO_2 generation of 49.6 kg CO_2, and the manufacturing of double-pane windows resulted in 76.05 kg CO_2. In the manufacturing of electrochromic glass windows, the float glass production process contributed 9.79 kg of CO_2 at that stage of fabrication. From the sensitivity analysis, it was determined that using 10% less electricity during electrochromic window production can lower carbon emissions for electrochromic windows by 1.51 kg CO_2. These life cycle assessment impact results were later used for advanced AI-predictive modeling using Python's scientific ecosystem, including PyTorch for neural network implementation, scikit-learn for data preprocessing and metric calculation, and custom-built hierarchical architectures to develop both Artificial Neural Network and Adaptive Neuro-Fuzzy Inference System models. Considering that 200 m^2 of double-pane windows were replaced by electrochromic windows, the embodied impact of electrochromic window production would be offset by the operational impact of 30.1 t CO_2 in 10.5 months. Since the lifespans of both window types are similar, electrochromic windows are promising green alternatives to double-pane windows.

Received 31st July 2025
Accepted 21st October 2025

DOI: 10.1039/d5su00638d

rsc.li/rscsus

Sustainability spotlight

Life Cycle Assessment (LCA) is a critical tool for evaluating the environmental impacts of any product and pathway and their sustainability. On the other hand, electrochromic windows (EC) are now considered a new, energy-efficient technology by adjusting their tint in response to external conditions. Due to the lack of any LCA on EC windows, there was a need to ensure their sustainability throughout the production pathway, from raw material extraction and manufacturing to installation and operation, by comparing them to conventional windows, which helps manufacturers to identify areas where energy use, emissions, and resource consumption can be minimized. Furthermore, artificial intelligence (AI) can help to predict the future emissions and environmental impacts of the current pathways of any product, such as EC windows. AI models can analyze vast amounts of data, optimize material choices, and predict long-term sustainability outcomes, leading to more accurate and promising results for achieving a sustainable and more environmentally friendly approach.

Introduction

Electrochromic (EC) windows can significantly reduce the amount of electricity required for lighting, heating, and cooling in buildings. Electrochromic layers on indium tin oxide (ITO)-coated glass enable manual or programmable control of the window's opacity. In the most common device architecture, applying a small electrical charge to the electrochromic layers causes lithium ions to transfer from one electrode to another, which in turn allows for redox switching of one or more electrochromic materials, which results in window tinting.[1] By reversing the polarity of the applied voltage, the opposite reactions occur, and the window lightens. By increasing the opacity of a window at certain times of the day, the amount of sunlight and heat can be reduced without the use of curtains or blinds.[2] The implementation of EC windows thus reduces energy costs for lighting, heating, and cooling in buildings.

[a]Department of Mining and Metallurgical Engineering, Mackay School of Earth Sciences and Engineering, University of Nevada, Reno, NV, 89557, USA. E-mail: evahidi@unr.edu

[b]Department of Civil and Environmental Engineering, University of Nevada, Reno, NV, 89557, USA

[c]Department of Chemistry, University of Nevada, Reno, NV, 89557, USA

[d]Department of Computer Engineering, Medipol University, Istanbul, 34810, Turkiye

[e]Aleon Metals, 302 Midway Rd., Freeport, TX, 77542, USA

Open Access Article. Published on 27 October 2025. Downloaded on 1/13/2026 2:20:04 AM.
This article is licensed under a Creative Commons Attribution-NonCommercial 3.0 Unported Licence.

In developed countries, buildings can account for up to 40% of total energy consumption in terms of carbon emissions.[3] Medium- and large-office buildings are particularly vulnerable to unnecessary energy consumption due to their high ratio of windows to square footage. Up to 64% of a building's energy consumption is due to a combination of lighting, heating, and cooling.[4] These energy costs contribute significantly to global warming. Implementing EC windows can help achieve net zero, LEED (Leadership in Energy and Environmental Design) building criteria, and Passive House sustainable building targets. Air conditioning energy consumption can be reduced by up to 50% compared to external shading, depending on the local climate, the building's glass-to-wall ratio, and its usage. Additionally, lighting energy can be reduced by up to 60% due to retained visibility through the window and the ability to control the level of shading, as opposed to window curtain or blind use.[5]

Due to the technologically advanced nature of EC windows, the environmental and financial costs of manufacturing and installation are considerably higher than those of double-pane (DP) windows. An EC window costs between \$550 and \$1600 per square meter of glass. The setup process of EC windows requires the installation of physical glass and frame, as well as the installation of frame cables, which are necessary for the electrical control of the window. DP windows cost between \$350 and \$950 per m^2 of glass. These estimates both include installation costs, albeit EC windows require more time and money to install due to the electrical components. EC and DP windows are structurally similar and are packaged as insulated glass units (IGUs). IGUs have multiple glass panes separated by a space filled with a noble gas and sealed to prevent condensation buildup, thereby improving insulation characteristics. IGUs have an average lifespan of 10 to 20 years, during which the seal and insulation are likely to become less effective.[6] EC windows can functionally change opacity for up to 30 years, assuming the window is cycled five times daily.[7] However, the seals in the IGU structure of the EC window typically fail before then. Considering all these benefits, the environmental impacts of EC windows have not been evaluated recently. On the other hand, artificial intelligence (AI) can facilitate not only assessing all potential aspects of the environmental profile but also accurately predicting it by considering all materials/energy flow inputs to the process.[8–10]

Therefore, the research will address the existing gap in the environmental impact of EC window production and demonstrate the long-term benefits of producing and implementing these windows, in direct connection to the environmental profile of DP windows. The manufacturing process of EC windows and the operational use of these windows were analyzed using a life cycle assessment (LCA) and an analysis of CO_2 emissions, respectively. Additionally, AI was used to ensure that all inputs into the process were taken into account.

Methodology

Goal and scope

System boundary and functional unit. This study investigates and compares the environmental impact of producing EC and conventional DP windows. The operational impact and energy savings to offset the production impact of EC windows are analyzed. The functional unit that establishes the reference flow of input and output of the system boundary is 1 m^2 of EC and DP window units. According to the ISO 14040 standard for LCA methodology, which was used for conducting this research, the standard LCA approach includes four steps: scope definition, life cycle inventory analysis, life cycle impact assessment, and interpretation.[11] The system boundary of the current study is shown in Fig. 1.

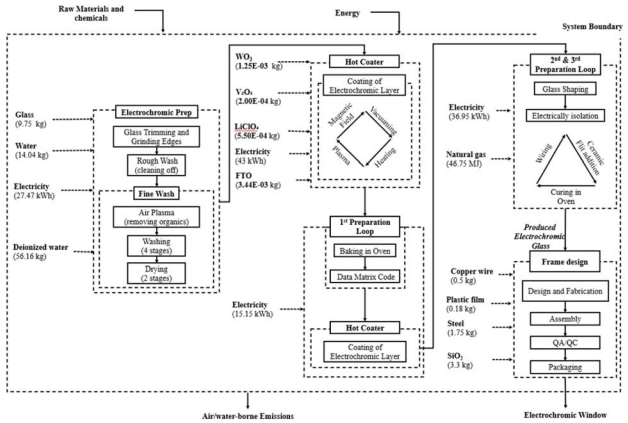

Fig. 1 Simplified system boundary to produce a 1 m^2 EC window (no wastes and co-products considered).

The LCA was conducted based on the Cut-Off, U, to assign burdens only to the initial production process or allocate them to waste treatment, rather than the product itself. The materials and energy volumes required to produce an EC window are outlined in Tables S1–5, grouped according to the six main production stages. The inputs include both the materials and energy requirements in terms of electricity and natural gas for the respective production stages and units. The overall output is 1 m^2 of an EC window. Like Syrrakou *et al.*, due to the lack of data on EC window production, data gathering was done considering different ways and similar products.[12]

Conventional DP window. The inventory for the life cycle assessment of producing 1 m^2 of a conventional argon-filled DP window is presented in Table S6. The production is considered a complete unit, and the inputs covered to enable comparative analysis with the EC window include the materials and energy requirements (electricity and natural gas).

Artificial neural networks (ANNs). Artificial neural networks (ANNs) are computational models developed to emulate the human brain's system of processes. Artificial neurons comprise the network, which collectively processes and learns from data to add pattern recognition and solve problems across machine learning, deep learning, and AI.[13] Artificial neurons are supposed to mimic the way human biological neurons process signals in ANNs. This entails receiving an input, applying weight coefficients and bias terms, executing it through an activation function, and forwarding the result to the following layer of neurons.[14]

 © 2025 The Author(s). Published by the Royal Society of Chemistry

Open Access Article. Published on 27 October 2025. Downloaded on 1/13/2026 2:20:04 AM.
This article is licensed under a Creative Commons Attribution-NonCommercial 3.0 Unported Licence.

The model is constructed using a feed-forward artificial neural network (FNN). This aligns with a training-based predictive model designed for regression-oriented tasks. For instance, for the case study of one of the stages in EC glass production, in particular "Electrochromic preparation", the following energy and materials are input to our model: float glass, water, and electricity. Additionally, there are environmental impacts. The model uses the following mean squared error formula as the loss function.

$$\mathrm{MSE} = \frac{1}{n}\sum_{i=1}^{n}(y_i - \hat{y}_i)^2 \tag{1}$$

where (y_i) represents the actual values from the output in the dataset, while on the other hand, $(\hat{y}_i)$ shows the predictive values that the model will extrapolate. The following procedure outlines the steps the formula follows.[15] For each data point (i), the model computes the difference between the actual value and the predicted value, squares this difference to subjugate larger errors, and then sums these squared differences across all (n) samples.[16,17] Finally, the total is divided by n, which is the number of observations, to obtain the average squared error across the dataset. The error metrics of RMSE, R, and MAPE% are also applied to test the validity and quality of the ANN model predictions and the TRACI-assessed outputs:

$$\mathrm{RMSE} = \sqrt{\frac{1}{n}\sum_{i=1}^{n}(y_i - \hat{y}_i)^2} \tag{2}$$

$$R = \frac{\sum_{i=1}^{n}(y_i - \bar{y})\left(\hat{y}_i - \bar{\hat{y}}\right)}{\sqrt{\sum_{i=1}^{n}(y_i - \bar{y})^2}\cdot\sqrt{\sum_{i=1}^{n}\left(\hat{y}_i - \bar{\hat{y}}\right)^2}} \tag{3}$$

$$\mathrm{MAPE} = \frac{100\%}{n}\sum_{i=1}^{n}\left|\frac{(y_i - \hat{y}_i)}{y_i}\right| \tag{4}$$

To ensure reproducibility and minimize overfitting, inputs were normalized using MinMax scaling, and random seeds were set for both NumPy and PyTorch.

Adaptive neuro-fuzzy inference system (ANFIS). The adaptive neuro-fuzzy inference system (ANFIS) is a hybrid system that integrates ANNs with the reasoning of human-like ability of fuzzy logic systems (FLS) concerning its ability to learn data. The primary operations of ANFIS involve mapping the inputs in terms of membership functions and a collection of fuzzy inference rules to forecast the outputs. The parameters are set using training data, typically, but not always, through one of the methods, such as backpropagation or hybrid learning algorithms.[18] ANFIS has two significant kinds of fuzzy inference systems: the Mamdani-type and the Takagi–Sugeno-type (or Sugeno-type) FIS. The Mamdani system is characterized by its language rule output and interpretability. In contrast, the Sugeno system is more favored in ANFIS, as it can be computationally efficient and better adapted to adaptive techniques, since it uses polynomial functions in the consequent part of the rules.[19] ANFIS typically employs the Sugeno-type FIS due to its mathematical consistency and its integration with optimization and learning methods.[20]

The basic architecture of ANFIS is a five-layer feed-forward network. The input values are first fuzzified using the fuzzification layer. The second layer is account-encoded processing, where the processing is performed in terms of a set of rules (typically fuzzy rules, often derived from Takagi–Sugeno). The third layer computes the firing strengths of these fuzzy rules by adjusting the firing strength between the input data and the fuzzy conditions for each rule. The difference is that the fourth layer produces all subsequent parameters (the outputs of each rule). The 5th equation, which is applied for computing the summation of those results to make the final result, is the next state.[19] In Fig. 2(a), this overall structure can be seen.

Although these models are capable of capturing nonlinear relationships well, they experience a similar loss of performance at high-dimensional input due to the exponential growth of fuzzy rules when a large number of input variables come into play. The "curse of dimensionality" results in computational inefficiency and overfitting. A straightforward yet effective means to circumvent this problem is to cluster the data. The idea is to group similar input variables into clusters, enabling the ANFIS model to evaluate a smaller number of input combinations effectively. For example, twelve input variables could be clustered into six groups, then into three groups, and ultimately into one output through hierarchical stages, which

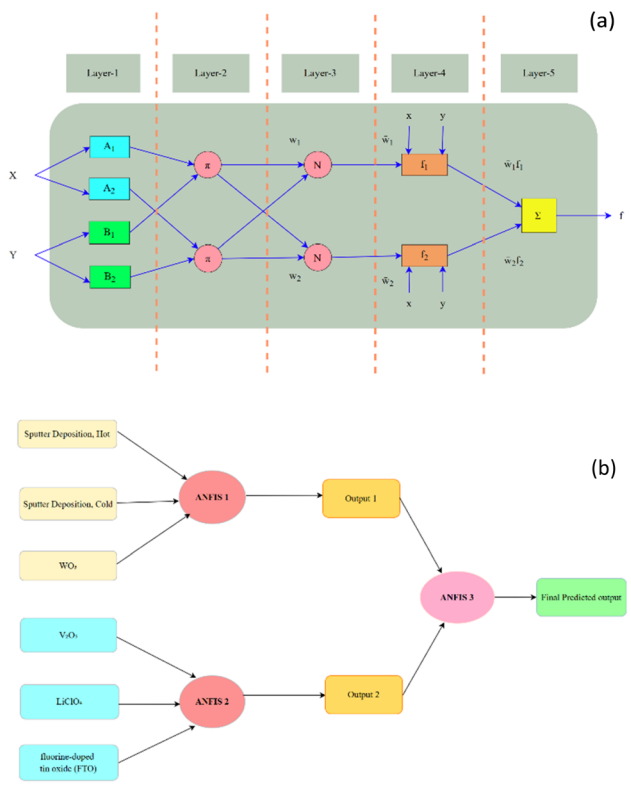

Fig. 2 (a) Visual representation of ANFIS's five-layer architecture with input datasets and a final output, and (b) multi-level ANFIS's visual demonstration of the Hot Coater stage's final predictions.

Open Access Article. Published on 27 October 2025. Downloaded on 1/13/2026 2:20:04 AM.
This article is licensed under a Creative Commons Attribution-NonCommercial 3.0 Unported Licence.

creates model complexity reduction and allows the model to scale effectively. With a group, the group can be assigned to its own ANFIS subnetwork, and the outputs can be summed together to create an overall prediction, which also allows manageable rule generation and better generalization.[21]

The structure shown in Fig. 2(b) suggests that the input data is composed of several material types, which can also be expanded to include input parameters such as process conditions, material type, and chemical composition. In this case, those inputs would be clustered (*e.g.*, by function or material type) and fed into different ANFIS subnetworks. If six distinct inputs were present, they could be grouped into three clusters, then into two, and eventually into one final model, forming a layered, modular system of ANFIS units. This hierarchical clustering approach enables the system to scale up while keeping the number of fuzzy rules in each subnetwork within a feasible range, making complex environmental impact modeling both accurate and computationally efficient.[21]

Just as the ANN model is assessed, the quality of the ANFIS model is also validated using the error metrics of RMSE, R, and MAPE%. The models are coded using Python's deep learning library, PyTorch, which utilizes the datasets of input and output data from EC production to generate predictions.

Results and interpretation

Life cycle inventory analysis

The inventory EC window production pathway. Fig. S1 displays the main stages of EC window production. The production of EC windows begins with the manufacturing of insulating glass units, which in this study are made from float glass. Float glass is a sheet of glass made from molten glass formed over a bed of molten metal of low melting point, typically a tin alloy.[22] A slightly reducing environment is maintained in the float chamber to avoid oxidation and unwanted reactions. The glass may spread uniformly at the high entrance temperature, smoothing uneven surfaces and creating a flat ribbon on the liquid metal bath. Conveyor rollers are used to draw ribbons continuously. At the same time, it cools over the tin alloy bath, reaching a temperature of roughly 1100 °F (590 °C), which permits it to be lifted without deformation or damage. The ribbon is then trimmed to size after being annealed to relieve stress. Through this method, flat glass with consistent thicknesses ranging from 2.5 mm (0.1″) to more than 25 mm (1″) is produced.[23]

In the manufacturing plant, the float glass is cut to the final size after which it is subjected to electrochromic processing. The glass is washed roughly first to remove all the cutting debris and then washed again in a fine way to remove finer particles. Air plasma is also applicable in the fine wash to clean organic contaminants on the glass surface. The glass is then subjected to four cleaning steps using clean water. Lastly, the float glass is dried twice to prepare it for the following process. The step eliminates all the particles of water, which may pose a barrier to the electrochromic application.[24] This phase of production involves coating the electrochromic layers onto the glass units. The prepared glass is heated in a vacuum chamber. To form the WO_3 working electrode on FTO (fluorine-doped tin oxide) on glass, a vanadium(v) oxide (V_2O_5) counter electrode, and an electrolyte containing lithium perchlorate ($LiClO_4$), sputter deposition is utilized.[24–27]

The coated glass is transferred to the next step, where the laser stage comprises three different cutting steps, where laser cuts are made through the coater to the glass, enabling the correct functioning of the internal circuitry upon the introduction of electricity.[28] Cold coating is used after the laser cut stage to add the final layer of the electrochromic material. No extreme heat is used in this step, hence the name, though the temperature still reaches about 150 °C.[29]

The second and third production steps primarily involve patterning of the device to make the final EC window product. The P2 laser cuts the panel into individual window units, which will be broken out during thermal layer separation. Before adding wires and curing in the oven, the P3 laser electrically isolates the windows, making them functional electrochromic devices. The window unit is manually inspected for defects, scribed by a high-power laser, and broken out manually after going through the x and y breaker bars.[24] The window units are then inspected for edge defects and then laminated. The device is then cured in an autoclave under heat and pressure after the array of glass units is done. The unit is wired and sealed, ready to be framed.[23]

The external frame, which holds the unit together, is typically made of stainless steel and is designed and cut out ready for assembly. A copper pigtail wire connected through the frame to the internal circuitry allows the transfer of electric charges, which brings about the desired tinting effect, *i.e.*, the electrochromic effect.[30] The frame design and assembly stage precede the final quality checks and distribution of the EC windows for installation.

Conventional DP window pathway. Double-pane or double-glazing windows utilize two different sets of glass, with an air- or gas-filled space sealed between the pieces. There is an aluminum or composite spacer between these two pieces of glass. To boost thermal performance, the cavity may be filled with either air or various types of insulated gases, such as argon or krypton. The thermal performance of double-pane windows is enhanced over that of single-pane windows due to the addition of an air gap, spacers, and the type of glass employed, which may consist of plain float glass, tempered glass, or low-emissivity (low-e) glass, offering improved energy efficiency and UV protection. Even in low-e glass, it is primarily the layer of gas, or the gas trapped in the cavity, that provides the insulation and low heat transfer property to the double-glazed design. The design significantly reduces heat transfer through the window, maintaining a more consistent indoor temperature. However, it can also provide beneficial sound insulation, creating a quieter interior environment compared to single-pane window designs. The manufacturer of float glass units for a typical, argon-filled double-pane (DP) window will first smelt and refine the raw materials to form a bed of melted metal for its DP window units. Float glass is manufactured from raw materials such as silica sand, alumina, and soda, according to the Pilkington process.[22,31]

 © 2025 The Author(s). Published by the Royal Society of Chemistry

Open Access Article. Published on 27 October 2025. Downloaded on 1/13/2026 2:20:04 AM.
This article is licensed under a Creative Commons Attribution-NonCommercial 3.0 Unported Licence.

Depending on the desired glass type, the glass undergoes post-forming processes such as annealing, lamination, and tempering. The glass is then cut, trimmed, and washed. The spacer is cut to size and shape to fit between two glass panes.[32] A sealant is applied on the edges to hold the unit together and provide an airtight space within which the insulating air is filled. The space is then evacuated, followed by the injection of insulating gas. Secondary sealing is done to ensure the unit is air and watertight.[33] A frame typically made of wood or stainless steel is fabricated and assembled with a gas-filled unit. It then undergoes rigorous quality checks and is packaged for distribution.[32]

Environmental impact assessment in the EC window production pathway

Electrochromic preparation. The contribution of process energy and materials in the electrochromic preparation step is illustrated in Fig. S2. All environmental categories are primarily dominated by flat glass production, followed by electricity used in substrate preparation, the application of electrochromic layers, and electrode integration. These steps are performed using automatic robots/machinery, where electricity is needed to produce high-quality EC windows.[34]

Hot coater stage. As shown in Fig. S3, cold or hot sputter deposition has an equal environmental impact across all categories. The main reason for high electricity usage in this step is related to the plasma-assisted deposition for the electrochromic layer, where a high-voltage electrical field is applied to create plasma.[24] Additionally, other chemicals used in this step had varying impacts on different categories, such as the significant impact of V_2O_5 on the smog and acidification categories.

First preparation loop. The effect of all materials/energy flows in the first preparation loop is displayed in Fig. S4. The electricity used in the oven for heating was the primary ingredient in this step, dominating all environmental categories. The oven is used to either facilitate the drying process or heat the coating substrates to enhance the properties of the applied electrochromic layer.[35] Therefore, electricity consumption during this step results in significant environmental impacts.

Second and third preparation loops. The resultant environmental effect of every material and energy flow on both the second and third loops of preparation is shown in Fig. S5. The findings indicate that the inputs that occupy the highest place in the overall environmental category include electricity and natural gas. Indicatively, an example of grinding and edging, and cleaning and surface preparation, where electricity is used, provides a significant contribution to all the categories of the environment. This powerful influence of electricity is the result of the electricity sources of production.[36] In one instance, the generation of electricity using fossil fuels has more environmental impacts than renewable sources.[37]

Frame design. Fig. S6 displays the environmental impact resulting from material and energy flows during the frame design stage. The silicon dioxide gel had the most significant environmental impact, followed by stainless steel and copper wire. The significant environmental impact of the silicon dioxide gel was due not just to the sodium silicate production process, but also the benchmark chemical process required to yield high-purity silicon dioxide gel.[38] Also, environmental impacts associated with stainless steel arise from its intense energy-consuming process, dust emissions into the air, landfill waste, and water discharge during its production.[39,40] The high impact of stainless steel on carcinogens stems from the use of nickel and chromium in stainless steel manufacturing.[41,42] Copper wire production, another prominent contributor, has unique environmental impacts resulting from mining, copper production, and the wiring process, requiring significant amounts of energy, raw materials, and land use. All of these lead to greenhouse gas emissions, air/water pollution, soil erosion, and habitat destruction.[43] However, it is possible to recycle copper to reduce its environmental impacts, both embodied and operational.[44]

Contribution of stages to the whole EC window production process

Due to the different environmental impacts resulting from various stages in the EC window production pathway, it was interesting to determine the contribution of each stage to the overall environmental profile. Fig. 3 shows the stepwise contribution of any stage of the EC window manufacturing process to the entire environmental profile. The frame design step contributes to all environmental categories. For example, approximately 60% of ecotoxicity is attributed to the frame design step.

Moreover, the frame design, followed by the second and third preparation loops, electrochromic preparation, and the hot coater stage, were other steps that made significant contributions. As mentioned earlier, these significant environmental impacts result from the electricity used in these steps.

Conventional DP window. The environmental impacts of the materials and energy flows in the production of a typical argon-filled stainless steel frame DP window are presented in Fig. S7. Aluminium is the highest contributor across almost all impact categories. The production of aluminium is energy-intensive,

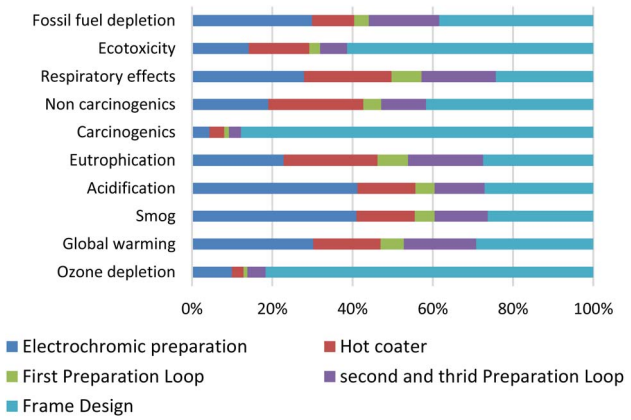

Fig. 3 Stepwise contribution of environmental impacts of stages to the whole environmental profile for the EC window manufacturing pathway.

Open Access Article. Published on 27 October 2025. Downloaded on 1/13/2026 2:20:04 AM.
This article is licensed under a Creative Commons Attribution-NonCommercial 3.0 Unported Licence.

considering the involved processes like electrolysis and alumina refining.[45] This is also accompanied by the release of CO_2, thereby increasing its environmental impact. This is minimal when aluminium is sourced from recycled products. Previous researchers have corroborated this[46] and have determined that recycling is the more environmentally friendly option.

Notably, the silica gel desiccant category is impacted by ozone depletion, which is generally achieved by acidifying a silicate solution, such as water glass. This reaction leads to the release of sulphur dioxide gas, which has a ripple effect on ozone depletion.[47] Soda, adhesives, and vinyl have significant impacts across all impact categories. The remainder is attributed to the energy impact of the high amounts of electricity and natural gas required to produce float glass for stages such as melting, annealing, and tempering.

Comparison. Most relevant to this study is the impact of the two types of windows on global warming. The analysis yields 49.6 kg of CO_2 equivalent in the production of the EC window, while the DP window generates 76.05 kg of CO_2, representing about 1.5 times that of the former, as shown in Fig. 4. The environmental impacts resulting from the conventional windows were higher in all environmental categories.

The reason synthetic materials (such as vinyl and polypropylene) are more ecotoxicologically relevant is that they are in other ways more ecotoxicologically hazardous. They are non-biodegradable; as a result, they will take a long time to decompose and generate durable areas of pollution, such as environmentally hazardous waste, which will have a material impact on plants and animals. Aluminium, which is used as a spacer material in DP windows, is absent in EC windows, and is one of the metals that consumes a high amount of energy in its production.[48] In a work by Zhang *et al.*[49] regarding the environmental footprint of aluminium production in China, aluminium production is accompanied by CO_2 and methane emissions, which contribute to global warming, as well as nitrogen oxide gas, which significantly impacts terrestrial acidification and respiratory health. These findings were consistent with the high aluminium impact observed in the production stage and its contributions, resulting in overall higher impacts in the ecotoxicity, carcinogenicity, eutrophication, respiratory effects, and acidification impact categories.

Sensitivity analysis. To conduct a comprehensive LCA study in accordance with ISO 14040, a sensitivity analysis was performed to assess the reliability and uncertainty of the results. In this regard, the primary input, electricity, has significant environmental impacts throughout the entire process. The sensitivity analysis results for three environmental categories of ozone depletion, global warming, and fossil fuel depletion are displayed in Fig. 5, showing ±10% change in inputs. The results showed that a 10% decrease in electricity led to a 1.51 kg CO_2 eq reduction in the global warming category, equivalent to approximately a 3% decrease in CO_2 emissions.

ANN results. The assessment of the predictive outputs from an ANN model based on PyTorch, relative to the five stages of the electrochromic glass supply chain, reveals sizable differences in environmental impacts based on stage and material selection. The ANN outputs presented in Table S7 show that the electrochromic preparation stage produces the maximum global warming potential (9.72 kg CO_2 eq) and maximum smog formation (1.03 kg O_3 eq) from float glass, but de-ionized water is identified as the least impactful throughout most of the environmental categories.[50,51] Table S9 indicates that during the hot coater stage, sputter deposition processes (both hot and cold) generate the highest global warming potential (2.52 kg CO_2 eq) and ecotoxicity impacts (30.3 CTUe). At the same time, the fluorine-doped tin oxide coating exhibits minimal environmental impact across most categories. Table S11 reveals that in the first preparation loop stage, the oven process generates substantially higher impacts than laser-based data matrix coding, particularly in terms of global warming (0.162 *vs.* 0.030 kg CO_2 eq) and fossil fuel depletion (1.80 *vs.* 0.031 MJ surplus).

As shown in Table S13, the second and third stages of the preparation loop involve glass cutting and grinding/edging, which are similar processes, and they have the most significant impact on global warming (1.03 and 1.76 kg CO_2 eq, respectively). Meanwhile, the assembly and integration stages have relatively lower environmental burdens compared to all

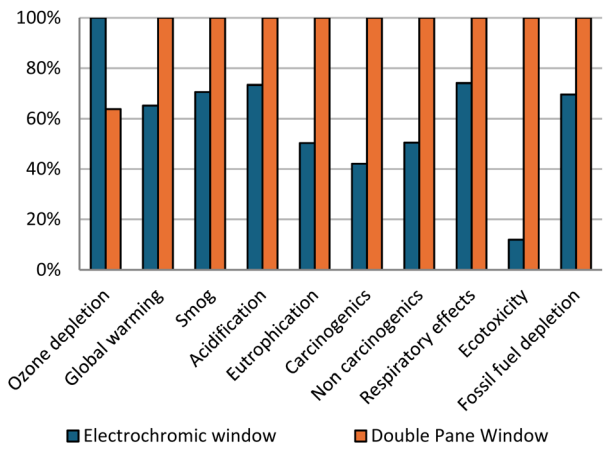

Fig. 4 A comparison between EC windows and DP windows based on the environmental impacts resulting from the production of 1 m^2 of them using TRACI.

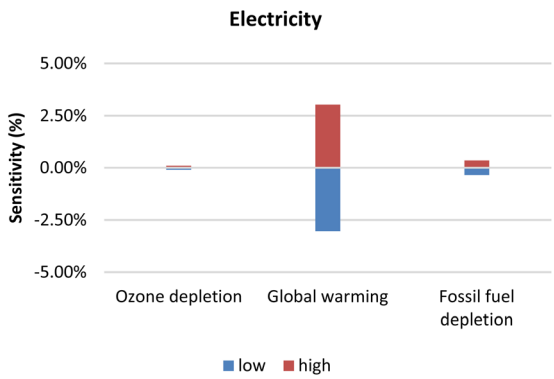

Fig. 5 Sensitivity analysis results indicate that electricity usage in the whole process is the primary contributor to high environmental impacts.

 © 2025 The Author(s). Published by the Royal Society of Chemistry

Open Access Article. Published on 27 October 2025. Downloaded on 1/13/2026 2:20:04 AM.
This article is licensed under a Creative Commons Attribution-NonCommercial 3.0 Unported Licence.

impact categories. Table S15 shows that, in the frame design loop, silicon dioxide gel has environmental impacts across all categories, with the highest impacts being specifically in global warming (10.39 kg CO_2 eq) and ecotoxicity (117.45 CTUe). Lastly, plastic film (polypropylene) has the lowest environmental burden overall, indicating that material selection is a crucial factor in determining the environmental performance of electrochromic glass production systems.

The ANN model demonstrated varied performance in predicting the eco-impact at five stages of electrochromic glass manufacturing and across three categories of impact assessment. In the case of electrochromic preparation stages (Tables S7 and S8), the overall correlation ranged from poor ($R = 0.195$ for respiratory impacts) to moderate-good ($R = 0.761$–0.774 for smog and acidification), with RMSE values remaining low (5.04×10^{-3}–3.14×10^{1}), indicating a reasonable prediction of output levels.[52,53] In the case of hot coater stages (Tables S9 and S10), R-values ranged from poor (0.208 for acidification) to excellent (0.990 for eutrophication), and RMSE values were relatively low (1.88×10^{-4}–1.93×10^{1}). However, MAPE was higher for some categories.

At stage one of the preparation loop (Tables S11 and S12), the model predicts all environmental impacts with great accuracy ($R = 1.00$), as well as low RMSE (1.14–14.6) and MAPE values, confirming accurate predictions. For stage two and three of the prep loop (Tables S13 and S14), the aggregate R values showed moderate overall prediction performance, ranging from −0.323 (ecotoxicity) to 0.993 (fossil fuel depletion), with only a few outputs poorly predicted; RMSE (3.08×10^{-4}–7.41×10) and MAPE (2.72–261) values were reasonable. At the frame design stage (Tables S15 and S16), most impact categories are predicted with accuracy, including global warming ($R = 1.00$) and smog formation ($R = 1.00$), while impacts like fossil fuel depletion ($R = -0.799$) and carcinogenics ($R = -0.185$) are not predicted nearly as well. Overall, the chosen ANN model successfully captures absolute and relative environmental impacts across all stages with a moderate level of confidence; that confidence is more pronounced when $R > 0.5$, RMSE is low, and the MAPE is considered an acceptable value; collectively, these metrics provide a slightly reliable basis for lifecycle impact analysis.[54]

All stages' contributions to all impacts have shown some interesting information based on Fig. 6. For example, the frame design manifested the most significant contribution associated with a number of environmental impact categories (fossil fuel depletion, ecotoxicity, respiratory effects, and acidification). Additionally, the electrochromic preparation stage made the most significant contribution to smog formation (approximately 60%) and significantly contributed to the impacts of acidification and fossil fuel depletion. This was also supported by findings from Wang *et al.*[55] who found that coating processes made a substantial contribution to the environmental effects in advanced glazing systems.

The first preparation loop, specifically, utilizes the impacts of carcinogens and non-carcinogens (almost 100%), indicating that this phase includes materials or processes of toxicological relevance. Although the hot coater phase displays relatively

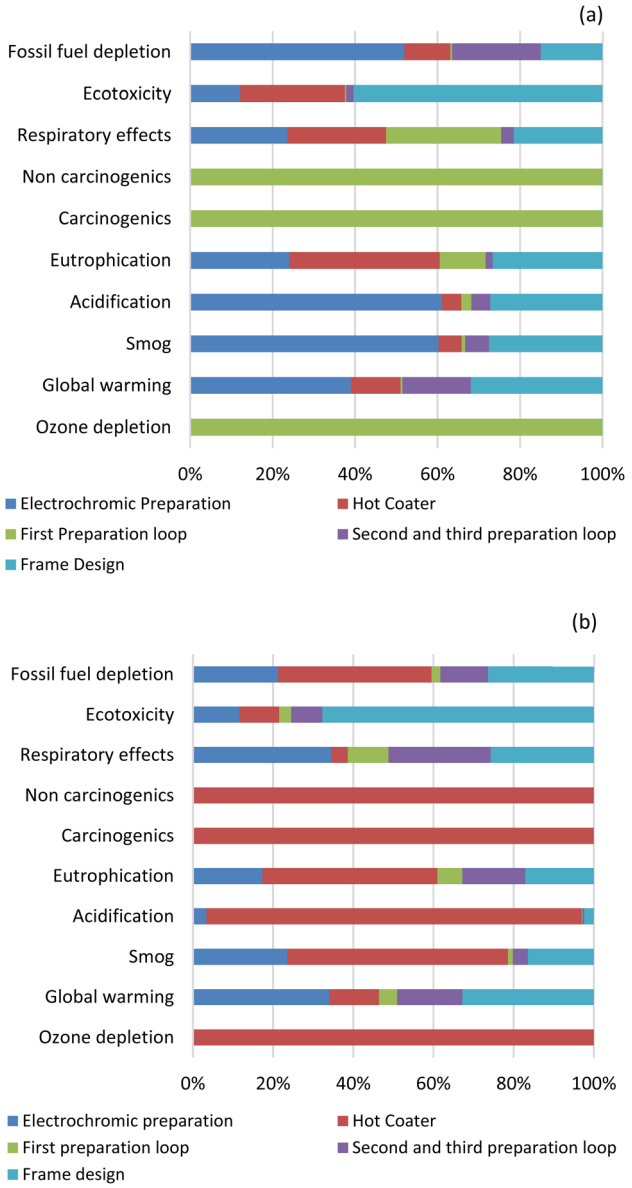

Fig. 6 Contribution of process energy and material flows in all stages of 1 m^2 EC glass production using (a) PyTorch's ANN model and (b) PyTorch's three-level ANFIS model.

lower error metric values in Table S10, its overall environmental impacts were balanced against those of other phases in the product system module and were primarily related to respiratory effects, eutrophication, and global warming. This trend was also observed in energy-dense thermal processes, as discussed by Lamnatou *et al.*[56] and Feizizadeh *et al.*[57] in the context of advanced materials processing systems.

Multi-layer ANFIS results. The ANFIS modelling approach, applied in PyTorch, reveals variations in environmental impact across different stages of electrochromic glass production.[58] The preparation stage for electrochromic coating (Table S17) shows that float glass is the most environmentally disadvantageous material, with global warming impacts of 10.1 kg CO_2 eq and ecotoxicity impacts of 77.6 CTUe. In contrast, water has

Open Access Article. Published on 27 October 2025. Downloaded on 1/13/2026 2:20:04 AM.
This article is licensed under a Creative Commons Attribution-NonCommercial 3.0 Unported Licence.

a very low environmental impact across most indicators. The hot coater stage (Table S19) uses sputter deposition methods, and in particular hot deposition methods, which have significant environmental burdens, contributing 30.5 kg CFC-11 eq to ozone depletion and 2.62 kg CO_2 eq to global warming overall, as opposed to the fluorine-doped tin oxide coat, which has negligible or no impacts on the environment across the vast majority of the categories that were studied.[59] The first preparation loop stage (Table S21) demonstrates a clear environmental benefit for laser data matrix (DM) coding over oven-based processing, with which the global warming contributions are both substantial (0.030 kg CO_2 eq *versus* 1.74 kg CO_2 eq), and the ecotoxicity effects are considerable (0.36 CTUe *versus* 21.0 CTUe). In the second and third preparation loop stages (Tables S23), glass cutting and grinding/edging contribute significantly to global warming impacts, at 1.31 and 1.79 kg CO_2 eq, respectively. At the same time, assembly and integration show relatively minor environmental impacts across most of the evaluated impact parameters.[60]

According to the frame design phase analysis from the three level ANFIS models (Table S25), silicon oxide gel would have the highest total environmental impacts across most TRACI categories (*e.g.* global warming: 9.99 kg CO_2 eq; smog: 0.625 kg O_3 eq; acidification: 0.469 kg SO_2 eq; respiratory impacts: 0.00932 kg PM_2.5 eq; fossil fuel depletion: 18.00 MJ) while polypropylene film would have the lowest total impacts at 0.55 kg CO_2 eq and 2.01 MJ, respectively. Ecotoxicity impacts were higher for copper wire (221 CTUe) than for stainless steel (144 CTUe), silicon oxide gel (111 CTUe), and polypropylene materials (4.92 CTUe). Normalized by total mass (reflecting consumption quantities in Table S5), global warming potentials are approximately 3.04 kg CO_2 eq per kg for polypropylene (0.55 ÷ 0.18 kg) *vs.* 3.02 kg CO_2 eq per kg for silicon oxide gel (9.99 ÷ 3.31 kg) and fossil fuel depletion about 11.17 MJ kg^{-1} *vs.* 5.44 MJ kg^{-1}, respectively.

The findings show that while the mass, which acts as the mass input of the silica gel, drives absolute stage impacts greater than those of polypropylene, the mass used for polypropylene would yield greater intrinsic impacts on a per-unit mass basis and hence emphasize the need to differentiate absolute environmental effects in relation to mass effects. The ANFIS model accurately captures trends, both in terms of absolute material impact and per-mass material impact, with low RMSE values and high correlations (Table S26), making it useful for understanding and further advancing insights into the environmental impacts of raw materials. The assessment of error metrics throughout the five stages of electrochromic glass production using ANFIS modelling shows considerable variation in prediction accuracy and overall model dependability. For electrochromic preparations (Table S18), the model performs exceedingly well, recording the highest values of correlation ($R = 1.000$) with almost all impact categories in all three ANFIS configurations. In contrast, the RMSE values remain incredibly low, from 1.000×10^{-8} to 33.2%, thus confirming extremely accurate predictions of environmental parameters.[55]

For the hot coater manufacturing stage (Table S20), we observe that the system performs very well in terms of prediction performance, with a perfect correlation coefficient of 1.000, which is the norm across all ANFIS models. There is, however, some variation in RMSE, which is evident in ecotoxicity and fossil fuel depletion issues, where reported values range from 1.64 to 47.2%.[61] In the first preparation loop phase (Table S22), we note great consistency out of the model with 1.000 *R*-values reported for all impact categories and ANFIS setups, which also report very low RMSE numbers that range from 1.00×10^{-6} to 8.21%; thus, we have very reliable model performance for that particular production step.[62] In the second and third preparation loop phases (Table S24), we observe good performance from different ANFIS configurations (ANFIS 1 through 7), which report correlation coefficients of 1.000 for most impact categories. Additionally, we observe RMSE numbers that, although ranging widely from 1.010×10^{-10} to 7.130×10^{-5}, still validate the model's ability to capture changes in environmental impact in these complex manufacturing processes.

The model performs exceptionally well in this final manufacturing phase, as the frame design phase (Table S26) reports very high predictive accuracy, with *R*-values of 1.000 for ozone depletion, global warming, smog, and many other impact categories. We also observe very low RMSE values, although occasionally ANIS 3 exhibits slightly off performance with *R* values that drop to nearly 99.8%, which is still within the trustworthy range. The three-level ANFIS model's overall contribution reveals different patterns of environmental effect distribution across the five stages of electrochromic glass production (Fig. 6). In particular, nearly all carcinogens and non-carcinogens are associated with the hot coater step, along with ozone depletion, indicating significant toxicological problems with sputter deposition.[63]

Due to its energy-intensive nature and material requirements, the electrochromic preparation stage contributes significantly to respiratory impacts, smog generation, and global warming (20–35% each). Due to the production of components such as silicon dioxide gel and metal frames, frame design is responsible for a significant portion (20–25%) of various impact categories, including ecotoxicity and the depletion of fossil fuels. Approximately 70% of the acidification impact is attributed to the hot coater stage, with electrochromic preparation accounting for a tiny portion of the total. It is surprising to learn that the initial preparation loop makes a significant contribution to respiratory impacts and eutrophication.

The depletion of fossil fuels and respiratory consequences, on the other hand, are primarily caused by the second and third preparation loops. Eco-design strategies for more sustainable electrochromic glass production could be informed by the potential optimization targets identified by this stage-specific environmental impact distribution, especially for toxic impacts in the hot coater stage and climate impacts in the electrochromic preparation stage.

ANFIS and ANN comparison. In terms of the coefficient of determination (R^2), the ANFIS model consistently outperforms the ANN approach in each of the five steps of the EC glass manufacturing process. For all environmental effect categories,

 © 2025 The Author(s). Published by the Royal Society of Chemistry

Open Access Article. Published on 27 October 2025. Downloaded on 1/13/2026 2:20:04 AM.
This article is licensed under a Creative Commons Attribution-NonCommercial 3.0 Unported Licence.

ANFIS has a perfect or near-perfect prediction capability ($R^2 \approx 1$) during the electrochromic preparation step (Fig. S18). On the other hand, ANN behaves poorly for respiratory impacts ($R^2 < 0.1$) but moderately for smog and acidification ($R^2 \approx 0.6$). ANN performs well in forecasting respiratory effects, carcinogenicity, and eutrophication ($R^2 > 0.9$), but struggles with projections for smog and acidification ($R^2 < 0.1$), according to the hot coater stage comparison (Fig. S19).

There was less linear variability during production compared to the preparation phase, as all categories' first preparation loop models were nearly perfectly fitted ($R^2 = 1$) (Fig. S20). Although the ANN architecture reached different performance levels ($R^2 < 0.1$) at the frame design stage, the ANFIS achieved perfect prediction scores for the second and third preparation loops (Fig. S21) and for the frame design stage (Fig. S22). This difference is consistent with earlier work that has shown ANFIS to perform better at modeling non-linear environmental systems, and with recent work showing that fuzzy-based models are superior to conventional ANNs in modeling complex manufacturing processes with uncertain parameters.[58,59]

Uncertainties and limitations in ANN/ANFIS-based LCA modelling. As with all predictive models, the predictions from the ANN and multi-level ANFIS models are subject to several sources of uncertainty. Overfitting was a specific concern for the models, particularly since the subnetworks are small and the number of stage-specific training data points is small. For ANFIS, the R values for the majority of impact categories lie between 0.999 and 1.000, which indicates a near-perfect fit on the training data. It is shown that for ANN, the R values between training and testing data vary from 0.195 to 0.987, depending on the stage and category. Some uncertainty in the results can arise from variations in raw material consumption and energy use across different life cycle stages, for example, for float glass, ranging from 9 to 57 kg and 10 to 28 kWh.

Predictive stability is also compromised by model sensitivity to hyperparameters (fuzzy rule counts, membership function variables, hidden layer numbers, epochs, and hierarchical clustering in ANFIS). At the same time, uncertainties stemming from the LCA inventory and characterization factors also transfer through the models (where global warming potentials range from \∼∼0.54–10.43 kg CO_2 eq and ecotoxicity impacts range from 5–220 CTUe between materials and construction stages \[stage-specific LCA datasets\]). Furthermore, scenario dependence complicates universality, as the trained models rely on the production conditions and material inputs from the training datasets. Thus, a better approach is to view model output as predictive approximations with uncertainty ranges, especially in light of the proven cross-validation efforts and sensitivity assessments, which provide added support for using ANN and ANFIS to investigate such sustainability-driven production patterns. These patterns ultimately still require tailored interpretation.

Operational energy consumption

After the windows are manufactured, they will be installed and utilized as energy-saving devices.[5] Prior studies have shown that the performance of EC windows is highly sensitive to building and climate parameters. For instance, according to a study in South Korea, EC windows reduce AC energy consumption by up to 50% and achieve a 60% reduction in lighting energy by using a window-to-wall ratio of 60%.[5] In another study done by Detsi *et al.* in 2024, it was found that 7–16% energy saving, leading to 18% cost reductions, can be achieved by using EC windows in warmer climates and high glazing ratios.[64] Furthermore, it has been reported that south-facing windows showed limited advantages compared to west-facing facades in Mediterranean climates.[65]

Table 1 Energy consumed in a 10 000-square-foot office building per year

Energy purpose	DP window consumption	EC window consumption	Units
Lighting	25 500	10 200	kWh
Cooling	16 500	8250	kWh
Heating	326 800	163 400	ft^3
Global warming impact	56 600	26 500	kg CO_2 eq

Based on these reports, considering four sunny days in different seasons, if EC windows replace 200 m^2 of DP windows in a 10 000 ft^2 medium office building, there is a possibility of significant energy savings. The energy saved by implementing EC windows can be converted to kg CO_2 eq and compared to the global warming contribution of their manufacturing. If 15 kWh of electricity and 38 ft^3 of natural gas are used per square foot of an office building, the total kg of CO_2 eq generated by lighting, cooling, and heating can be determined. This operates on the assumption that in a medium office building, approximately 17% of total electricity use is for lighting, 11% of total electricity use is for cooling, and 86% of total natural gas is used for heating. The difference in consumption is summarized in Table 1.

As anticipated, a medium-sized office building will consume less energy and therefore generate 30 100 fewer kg CO_2 eq when equipped with EC windows. 131.7 kg CO_2 eq is generated during the manufacturing process for every m^2 of EC windows. Therefore, it can be concluded that after 12 months of operation, the manufacturing global warming impact will be mitigated.

Conclusion

An LCA study was conducted to assess the environmental footprints of EC windows, using SimaPro 9.1. and Ecoinvent. TRACI 2.1. was used to evaluate the environmental impacts associated with various stages to produce 1 m^2 of EC windows. Based on results obtained from different stages, it was found that the frame production stage made the highest contribution to the overall process, accounting for approximately 33% of the total CO_2 eq (13 kg CO_2 eq) emitted from this step.

The results revealed that energy resources, including natural gas and electricity, contributed mainly to all environmental categories in all stages of the EC window production pathway.

Open Access Article. Published on 27 October 2025. Downloaded on 1/13/2026 2:20:04 AM.
This article is licensed under a Creative Commons Attribution-NonCommercial 3.0 Unported Licence.

Other prominent contributors with significant environmental impacts were stainless steel, copper wire, and alumina. Another LCA study was conducted for the environmental assessment of DP window production. The results showed that, in addition to energy resources, such as natural gas, there were other inputs, including alumina, soda, and silica gel, which had significant environmental impacts.

The impacts of the EC and DP windows were compared, and it was found that the EC window production pathway had higher environmental impacts in the categories of ozone depletion, global warming, smog, and fossil fuel depletion. On the other hand, the DP window showed higher environmental implications in the remaining categories, particularly in ecotoxicity. The sensitivity analysis on EC window production revealed that a 10% decrease in electricity usage throughout the process would result in a reduction of 1.51 kg of CO_2 eq per m^2. The majority of electricity and natural gas used in office buildings is due to lighting, cooling, and heating. The energy use for these variables can be reduced by implementing EC windows. In a 10 000 sq ft office building, it will take 10.5 months to offset the global warming impact of 200 sq m of EC windows.

The study's findings, which compare ANN and multi-level ANFIS models for predicting environmental impacts of electrochromic window development, illustrate apparent differences between the two systems. They both accurately assessed areas of concern related to this production process, demonstrating that float glass preparation components have a significant impact on global warming, with a total of 10.1 kg CO_2 equivalent. Meanwhile, silicon dioxide gel represents a substantial impact, with melting and refining impacts of 117.45 CTUe. In addition, the thermal coating process, particularly related to sputter deposition, is a significant environmental contributor, generating as much as 30.5 kg of CFC-11 equivalent ozone depletion potential alone over one production cycle. Ultimately, the model of multi-level ANFIS provides consistent results of high accuracy, as evidenced by correlation values of 1.000 in most impact assessment areas and stages of the production process. In contrast, the ANN model showed more variability, generating correlation coefficients from 0.195 to 0.987 depending on the areas of production and environment measured.

High environmental differences were caused by the choice of material, as evidenced by the low global warming potential of polypropylene plastic film (0.539 kg CO_2 equivalent) compared to the high global warming potential of silicon dioxide gel (9.99 kg CO_2 equivalent). The three-tier ANFIS model, with epoch settings ranging from 200 to 1000, demonstrated an outstanding ability to recognize complex environmental trends, with root mean square errors at or below 0.01 in most measurement classes. An analysis of errors revealed that ANFIS models had very low values of mean absolute percentage error, ranging from 0.18% to 48%. In comparison, ANN models were more inconsistent, ranging from 2.78% to 1.49×10^5, which represents the error depending on the manufacturing stage under investigation.

The impact of environmental differences across different stages of production processes was a significant 1.31 to 1.79 kg CO_2 equivalent of the global warming impact, which, relative to the activities of assembly and integration, was below 0.20 kg CO_2 equivalent. Lastly, though both methods of artificial intelligence gave similar guidance on the sustainability of the production, the multi-level ANFIS approach was found to be more credible due to the consistently high correlation coefficients higher than 0.999 and lower rates of error with a continuous production of the electrochromic window and with the multi-level ANFIS being the method of choice when analyzing the sustainability of the production process and establishing the needed parameters that must be met to consider the environmental impact in a certain way.

Author contributions

Mohsen Rabbani: design of the work for the LCA study, the acquisition, analysis, and interpretation of data for the different stages of the LCA study, and drafting the work. Olivia Tahti: the acquisition, analysis, and interpretation of data for different stages of this LCA study. Sabinus Essel Arthur: the acquisition, analysis, and interpretation of data for the different stages of the LCA study. Macy A. Hopping: evaluation of the database for the final inventory and stages, the acquisition, analysis, and interpretation of data for the different stages of the LCA study, drafting the work, and reviewing. Christopher J. Barile: drafting the work and reviewing the final draft. Mohd Hassan Karim: design of the work for the AI study, the acquisition, analysis, and interpretation of data for the AI study. Ario Fahimi: design of the LCA study, revision, and final evaluation. Ehsan Vahidi: drafting the work, reviewing, and supervising this LCA study.

Conflicts of interest

There are no conflicts to declare.

Data availability

The data supporting this article have been included as part of the supplementary information (SI). Supplementary information is available. See DOI: **https://doi.org/10.1039/d5su00638d**.

References

1 A. M. Ardakan, E. Sok and J. Niemasz, *Energy Proc.*, 2017, **122**, 343–348.
2 A. Cannavale, *Clean Technol.*, 2020, **2**, 462–475.
3 M. N. Mustafa, M. A. A. M. Abdah, A. Numan, A. Moreno-Rangel, A. Radwan and M. Khalid, *Renew. Sustain. Energy Rev.*, 2023, **181**, 113355.
4 D. Ürge-Vorsatz, L. F. Cabeza, S. Serrano, C. Barreneche and K. Petrichenko, *Renew. Sustain. Energy Rev.*, 2015, **41**, 85–98.
5 J. H. Kim, J. Hong and S. H. Han, *Sustainability*, 2021, **13**, 1815.

 © 2025 The Author(s). Published by the Royal Society of Chemistry

Open Access Article. Published on 27 October 2025. Downloaded on 1/13/2026 2:20:04 AM.
This article is licensed under a Creative Commons Attribution-NonCommercial 3.0 Unported Licence.

6 K. P. Munshi, *Analysis of life cycle costs and energy savings of electrochromic glazing for an office building*, Arizona State University, 2012.
7 N. C. Bhoumik, D. C. Madu, C. W. Moon, L. S. Arvisu, M. D. McGehee and C. J. Barile, *Joule*, 2024, **8**, 1036–1049.
8 G. U. Alaneme, K. A. Olonade, E. Esenogho, M. M. Lawan and E. Dintwa, *Sci. Rep.*, 2024, **14**, 26151.
9 G. U. Alaneme, K. A. Olonade and E. Esenogho, *Discov. Mater.*, 2023, **3**, 14.
10 E. Esenogho, K. Djouani and A. M. Kurien, *IEEE Access*, 2022, **10**, 4794–4831.
11 ISO 14040:2006, Environmental Management—Life Cycle Assessment—Principles and Framework, 2006.
12 E. Syrrakou, S. Papaefthimiou and P. Yianoulis, *Sol. Energy Mater. Sol. Cells*, 2005, **85**, 205–240.
13 G. R. Yang and X. J. Wang, *Neuron*, 2020, **107**, 1048–1070.
14 G. V. S. Bhagya Raj and K. K. Dash, *Crit. Rev. Food Sci. Nutr.*, 2022, **62**, 2756–2783.
15 I. Goodfellow, Y. Bengio and A. Courville, *Deep Learning*, MIT Press, 2016.
16 A. Géron, *Hands-on machine learning with Scikit-Learn, Keras, and TensorFlow*, O'Reilly Media, Inc., 2022.
17 C. M. Bishop and N. M. Nasrabadi, *Pattern recognition and machine learning*, Springer, New York, 2006.
18 S. O. Sada and S. C. Ikpeseni, *Heliyon*, 2021, **7**, e06136.
19 M. D. Pop, D. Pescaru and M. V. Micea, *Sensors*, 2023, **23**, 8791.
20 H. Nguyen, T. D. Bao, X. N. Bui, V. V. Pham, D. A. Nguyen, N. H. Do, *et al.*, *Nat. Resour. Res.*, 2025, 1–34.
21 Z. Zhang, M. Al-Bahrani, B. Ruhani, H. H. Ghalehsalimi, N. Z. Ilghani, H. Maleki, *et al.*, *Chem. Eng. J.*, 2023, **471**, 144362.
22 Q. Zhang, Z. Chen and Z. Li, *Appl. Therm. Eng.*, 2011, **31**, 1272–1278.
23 E. O. Lawrence, E. Worrell, C. Galitsky, E. Masanet, and W. Graus, *LBNL-57335-Revision*, 2008.
24 M. Burdis and N. Sbar, *Electrochromic Windows: Process and Fabrication Improvements for Lower Total Costs*, Sage Electrochromics, Incorporated, 2007.
25 S. H. Yang, J. H. Yang, Z. Y. Chen, and C. C. Ho, *Proceedings of the 7 th International Conference on Applied Innovations*, 2021, pp. 19–21.
26 N. Daroogheh, E. Karimi and S. M. B. Ghorashi, *Int. J. Opt. Photonics*, 2019, **13**, 79–88.
27 Y. Ke, Z. Wang, H. Xie, M. A. Khalifa, J. Zheng and C. Xu, *Membranes*, 2023, **13**(6), 601.
28 S. Nikumb, Q. Chen, C. Li, H. Reshef, H. Y. Zheng, H. Qiu, *et al.*, *Thin Solid Films*, 2005, 216–221.
29 M. Kamalisarvestani, R. Saidur, S. Mekhilef and F. S. Javadi, *Renew. Sustain. Energy Rev.*, 2013, **26**, 353–364.
30 R. Zheng, Y. Wang, J. Pan, H. A. Malik, H. Zhang, C. Jia, *et al.*, *ACS Appl. Mater. Interfaces*, 2020, **12**, 27526–27536.
31 M. L. F. Nascimento, *World Patent Inf.*, 2014, **38**, 50–56.
32 T. D. Nguyen, L. P. Yeo, A. J. Ong, Z. W. Wang, D. Mandler and S. Magdassi, *Mater. Today Energy*, 2020, **18**, 100496.
33 M. Arney, *Integrated energy efficient window-wall systems*, Aspen Research Corporation, 2002.
34 C. Baldassarri, A. Shehabi, F. Asdrubali and E. Masanet, *Sol. Energy Mater. Sol. Cells*, 2016, **156**, 170–181.
35 B. Deng, Y. Zhu, X. Wang, J. Zhu, M. Liu, M. Liu, *et al.*, *Adv. Mater.*, 2023, **35**, 2302685.
36 S. T. Huber and K. W. Steininger, *J. Clean. Prod.*, 2022, **339**, 130720.
37 M. V. Barros, R. Salvador, C. M. Piekarski, A. C. de Francisco and F. M. C. S. Freire, *Int. J. Life Cycle Assess.*, 2020, **25**, 36–54.
38 I. N. Pyagay, A. A. Shaidulina, R. R. Konoplin, D. I. Artyushevskiy, E. A. Gorshneva and M. A. Sutyaginsky, *Catalysts*, 2022, **12**(2), 162.
39 C. van Sice and J. Faludi, *Proc. Des. Soc.*, 2021, 671–680.
40 T. Liang, S. Wang, C. Lu, N. Jiang, W. Long and M. Zhang, *J. Clean. Prod.*, 2020, **264**, 121697.
41 L. Patnaik, S. R. Maity and S. Kumar, *Mater. Today Proc.*, 2019, 638–643.
42 P. Taxell and P. Huuskonen, *Regul. Toxicol. Pharmacol.*, 2022, **133**, 105227.
43 G. Izydorczyk, K. Mikula, D. Skrzypczak, K. Moustakas, A. Witek-Krowiak and K. Chojnacka, *Environ. Res.*, 2021, **197**, 111050.
44 T. Wang, P. Berrill, J. B. Zimmerman and E. G. Hertwich, *Environ. Sci. Technol.*, 2021, **55**, 5485–5495.
45 S. H. Farjana, N. Huda and M. A. P. Mahmud, *Sci. Total Environ.*, 2019, **663**, 958–970.
46 G. Grimaud, N. Perry and B. Laratte, *Procedia CIRP*, 2016, 212–218.
47 S. Selkowitz, R. Hart and C. Curcija, *Breaking the 20 Year Logjam to Better Insulating Windows*, Lawrence Berkeley National Lab. (LBNL), Berkeley, CA (United States), 2018.
48 G. Liu and D. B. Müller, *J. Clean. Prod.*, 2012, **35**, 108–117.
49 Y. Zhang, M. Sun, J. Hong, X. Han, J. He and W. Shi, *J. Clean. Prod.*, 2016, **133**, 1242–1251.
50 E. Syrrakou, S. Papaefthimiou and P. Yianoulis, *Sol. Energy Mater. Sol. Cells*, 2005, **85**, 205–240.
51 B. P. Jelle, A. Hynd, A. Gustavsen, D. Arasteh, H. Goudey and R. Hart, *Sol. Energy Mater. Sol. Cells*, 2012, **96**, 1–28.
52 N. Meinshausen and P. Bühlmann, *J. R. Stat. Soc. Ser. B*, 2010, **72**, 417–473.
53 P. Stolz, R. Frischknecht, F. Wyss and M. de Wild-Scholten, *PEF screening report of electricity from photovoltaic panels in the context of the EU Product Environmental Footprint Category Rules (PEFCR) Pilots v. 2.0*, Uster, Switzerland, 2016.
54 V. Fthenakis, *MRS Bull.*, 2012, **37**, 425–430.
55 T. Wang, Y. Zhu, P. Ye, W. Gong, H. Lu and H. Mo, *IEEE Trans. Comput. Soc. Syst.*, 2022, **11**, 101–116.
56 C. Lamnatou, J. D. Mondol, D. Chemisana and C. Maurer, *Renew. Sustain. Energy Rev.*, 2015, **48**, 178–191.
57 B. Feizizadeh, K. Mohammadzade Alajujeh, T. Lakes, T. Blaschke and D. Omarzadeh, *GISci. Remote Sens.*, 2021, **58**, 1543–1570.
58 K. Struhala and M. Ostrý, *J. Clean. Prod.*, 2022, **336**, 130359.
59 N. Kardani, A. Bardhan, D. Kim, P. Samui and A. Zhou, *J. Build. Eng.*, 2021, **35**, 102105.
60 M. K. Nematchoua, A. Yvon, S. E. J. Roy, C. G. Ralijaona, R. Mamiharijaona and J. N. Razafinjaka, *J. Energy Storage*, 2019, **24**, 100748.

Open Access Article. Published on 27 October 2025. Downloaded on 1/13/2026 2:20:04 AM.
This article is licensed under a Creative Commons Attribution-NonCommercial 3.0 Unported Licence.

61 U. Posset and M. Harsch, *Electrochromic Mater. Devices*, 2013, 545–570.
62 J. S. Jang, *IEEE Trans. Syst. Man Cybern.*, 1993, **23**, 665–685.
63 H. H. Tang and N. S. Ahmad, *Syst. Sci. Control Eng.*, 2024, **12**, 2394429.
64 M. Detsi, I. Atsonios, I. Mandilaras and M. Founti, *Energy Build.*, 2024, **319**, 114553.
65 P. F. Tavares, A. R. Gaspar, A. G. Martins and F. Frontini, *Energy Policy*, 2014, **67**, 68–81.

 © 2025 The Author(s). Published by the Royal Society of Chemistry